ACS APPLIED MATERIALS & INTERFACES

Research Article

Cite This: ACS Appl. Mater. Interfaces 2019, 11, 9747−9755

www.acsami.org

Biomineralization Synthesis of the Cobalt Nanozyme in SP94-Ferritin Nanocages for Prognostic Diagnosis of Hepatocellular Carcinoma

Bing Jiang,[†,‡,∥] Liang Yan,[§,∥] Jianlin Zhang,[†] Meng Zhou,[†] Guizhi Shi,[†] Xiuyun Tian,[§] Kelong Fan,*[,†] Chunyi Hao,*[,§] and Xiyun Yan*[,†,‡]

[†]Key Laboratory of Protein and Peptide Pharmaceuticals, CAS-University of Tokyo Joint Laboratory of Structural Virology and Immunology, Institute of Biophysics, Chinese Academy of Sciences, Beijing 100101, China

[‡]College of Life Sciences, University of Chinese Academy of Sciences, Beijing 100049, China

[§]Key Laboratory of Carcinogenesis and Translational Research, Department of Hepato-Pancreato-Biliary Surgery, Peking University Cancer Hospital & Institute, Beijing 100142, China

Supporting Information

ABSTRACT: Nanomaterials with intrinsic enzyme-like activities (nanozymes) have emerged as promising agents for cancer theranostics strategies. However, size-controllable synthesis of nanozymes and their targeting modifications are still challenging. Here, we report a monodispersed ferritin-based cobalt nanozyme (HccFn(Co_3O_4)) that specifically targets and visualizes clinical hepatocellular carcinoma (HCC) tissues. The cobalt nanozyme is biomimetically synthesized within the protein shell of the HCC-targeted ferritin (HccFn) nanocage, which is enabled by the display of HCC cell-specific peptide SP94 on the surface of ferritin through a genetic engineering approach. The intrinsic peroxidase-like activity of HccFn(Co_3O_4) nanozymes catalyzes the substrates to make color reaction to visualize HCC tumor tissues. We examined 424 clinical HCC specimens and verified that HccFn(Co_3O_4) nanozymes distinguish HCC tissues from normal liver tissues with a sensitivity of 63.5% and specificity of 79.1%, which is comparable with that of the clinically used HCC-specific marker α fetoprotein. Moreover, the pathological analysis indicates that the HccFn(Co_3O_4) nanozyme staining result is a potential predictor of prognosis in HCC patients. Staining intensity is positively correlated to tumor differentiation degree ($P = 0.0246$) and tumor invasion ($P < 0.0001$) and negatively correlated with overall survival ($P = 0.0084$) of HCC patients. Together, our study demonstrates that ferritin is an excellent platform for size-controllable synthesis and targeting modifications of nanozymes, and the HccFn(Co_3O_4) nanozyme is a promising reagent for prognostic diagnosis of HCC.

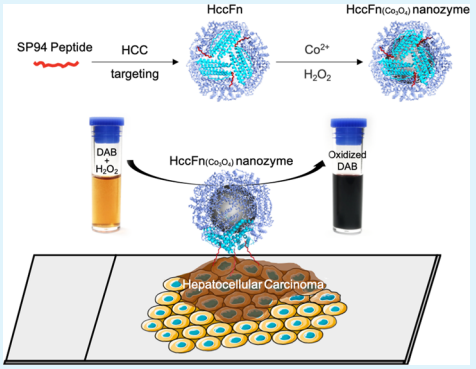

KEYWORDS: *HccFn(Co_3O_4) nanozyme, ferritin nanocage, SP94, HCC, prognostic diagnosis*

1. INTRODUCTION

Since an enzyme-like activity was discovered in Fe_3O_4 nanoparticles (NPs) in 2007,[1] the term "nanozyme" has been coined to describe nanomaterials with intrinsic enzyme-like activities,[2] typically exhibiting high tunable enzymatic activities. Moreover, they possess multiple functions, high stability, and are easily scaled up with low cost.[3,4] Considering the above advantages, nanozymes pose to be a superior alternative to natural enzymes or traditional enzyme mimetics in biomedical and biosensing applications. However, it is still challenging to synthesize nanozymes in a controlled manner with a constrained size distribution and targeting modifications until now.[5]

Using cage-like proteins as templates to synthesize nanomaterials has been demonstrated to be an efficient approach to produce uniform and monodispersed NPs.[6] Among them, ferritin, because of its self-assembly ability and unique spherical and symmetrical architecture,[7] has emerged as an excellent protein nanocage for metal[8−10] and metal oxide NP[11,12] synthesis. In addition, the ferritin nanocage is also suitable for surface modification by the genetic engineering approach.[13] Modified with targeting ligands, ferritin can be endowed with specific targeting abilities.[14,15] These characteristics make it easy for ferritin nanocages to synthesize ferritin-based nanozymes possessing specific targeting ability as well as monodispersity.

The first ferritin-based nanozyme possessing peroxidase-like activity was reported in 2012.[11] Fe_3O_4 NPs were biomimetically synthesized in the cavity of human heavy-chain ferritin. This novel kind of magnetoferritin (M-HFn) nanozyme

Received: November 28, 2018
Accepted: February 19, 2019
Published: February 19, 2019

DOI: 10.1021/acsami.8b20942
ACS Appl. Mater. Interfaces 2019, 11, 9747−9755

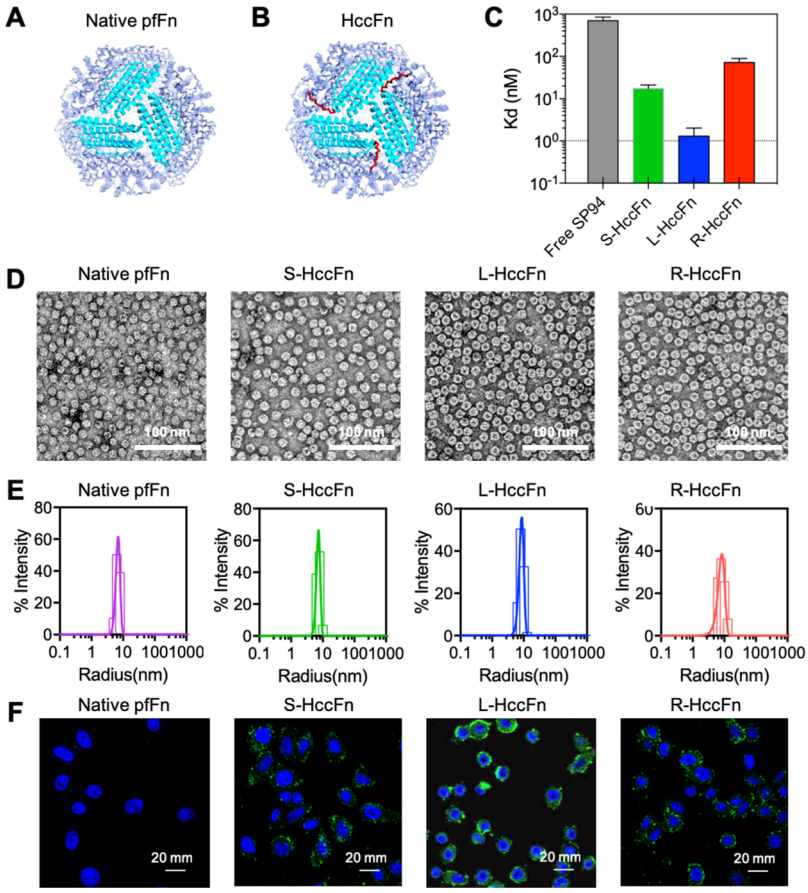

Figure 1. Characteristics of HccFn nanocages. (A) Schematic diagram of native pfFn nanocages. (B) Schematic diagram of HccFn nanocages. (C) Determination of the binding affinity of free SP94, S-HccFn, L-HccFn, R-L-HccFn, and HCC cell HepG2. (D) TEM images of native pfFn, S-HccFn, L-HccFn, and R-L-HccFn nanocages. (E) DLS analysis of native pfFn, S-HccFn, L-HccFn, and R-L-HccFn nanocages, with radius in solutions of 6.9, 7.5, 8.7, and 8.4 nm, respectively. (F) Confocal microscopy images of HepG2 cells after 30 min of incubation with FITC-labeled native pfFn and HccFn nanocages. Blue and green fluorescent signals represent 4,6-diamidino-2-phenylindole dihydrochloride (DAPI)-stained nuclei and FITC-labeled nanocages, respectively.

specifically targets and visualizes transferrin receptor 1 (TfR1)-positive tumor tissues. Unlike antibody-conjugated nanozymes, which are liable to mutually adhere and coagulate, resulting in poor dispersion and stability, ferritin-based nanozymes may be a better choice as a nanoprobe in immunohistochemical (IHC) assays[11] because of the monodispersity of ferritin. However, the peroxidase-like activity of the Fe_3O_4 NPs was relatively low compared with natural horseradish peroxide (HRP),[1] which limits the biomedical applications of ferritin-based nanozymes. Thus, improving the peroxidase-like activity of ferritin-based nanozymes may increase the sensitivity of tumor diagnosis, and provide more information about the pathological analysis of specimens. It was reported that Co_3O_4 NPs possess higher peroxidase-like activity than that of Fe_3O_4 NPs;[16,17] thus, Co_3O_4 NPs may be a better option for constructing ferritin-based nanozymes with higher peroxidase-like activity. Moreover, the pathological diagnosis of different types of tumors with prognostic information needs more types of biomarker-targeting strategies. Novel ferritin-based nanozymes with higher enzymatic activity and specific tumor-targeting property are needed.

It is reported that peptide SP94 specifically binds to hepatocellular carcinoma (HCC) cells[18] and is subsequently used for HCC diagnosis and therapy.[19−23] In this study, we rationally designed a new HCC-targeted HccFn(Co_3O_4) nanozyme, in which the SP94 peptide was modified onto the exterior surface of ferritin nanocage (HccFn), and the Co_3O_4 nanozyme was biomimetically synthesized in the cavity of HccFn. As human and mouse ferritin proteins have been reported to interact with several membrane proteins,[24−26] to guarantee the sole targeting ability of nanozymes to HCC, we chose *Pyrococcus furiosus* ferritin (pfFn) as structural motif to construct the HccFn(Co_3O_4) nanozyme. Moreover, we demonstrated that the HccFn(Co_3O_4) nanozyme is able to specifically target and visualize clinical HCC tissues. Using the HccFn(Co_3O_4) nanozyme-based HCC diagnostic method, we examined 424 clinical specimens from HCC patients and verified that HccFn(Co_3O_4) nanozymes distinguished HCC tissues from normal tissues with a sensitivity of 63.5% and specificity of 79.1%, which is comparable with that of the clinically used HCC-specific marker α fetoprotein (AFP).[27] More importantly, we found that the HccFn(Co_3O_4) nanozyme-based HCC diagnostic method possesses prognostic diagnosis ability. Thus, ferritin is an ideal nanocage to produce size-controllable and targeting modified nanozymes; in addition, the HccFn(Co_3O_4) nanozyme is a promising tool for HCC tumor prognostic diagnosis.

DOI: 10.1021/acsami.8b20942
ACS Appl. Mater. Interfaces 2019, 11, 9747−9755

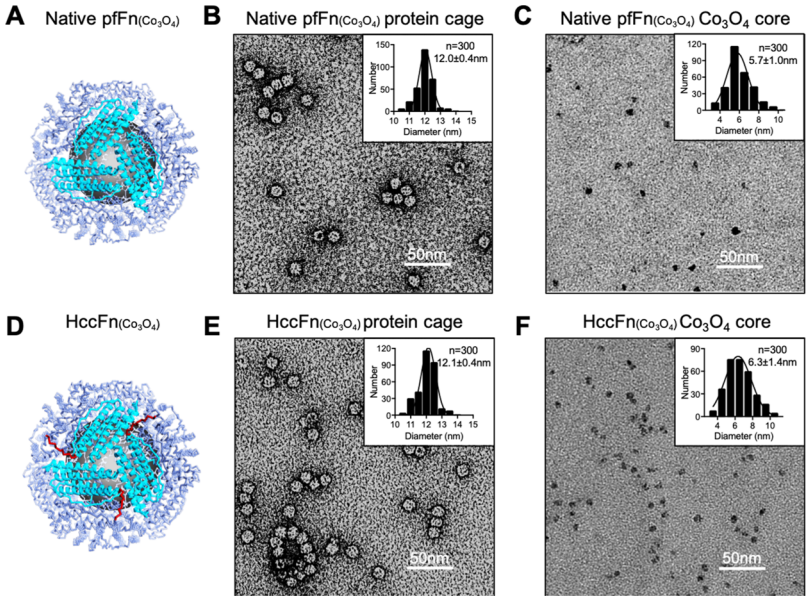

Figure 2. Characterization of HccFn(Co_3O_4) nanozymes. (A) Schematic diagram of native pfFn(Co_3O_4) nanozymes. (B) TEM image with negative staining and size distribution (inset diagram) of the protein cage of native pfFn(Co_3O_4) nanozymes. (C) TEM image without negative staining and size distribution (inset diagram) of the Co_3O_4 core of native pfFn(Co_3O_4) nanozymes. (D) Schematic diagram of HccFn(Co_3O_4) nanozymes. (E) TEM image with negative staining and size distribution (inset diagram) of the protein cage of HccFn(Co_3O_4) nanozymes. (F) TEM image without negative staining and size distribution (inset diagram) of the Co_3O_4 core of HccFn(Co_3O_4) nanozymes. The particle size was calculated by ImageJ software.

2. RESULTS

2.1. Synthesis and Characteristics of HCC-Targeting Protein Nanocage. The HCC-targeting protein nanocage (HccFn) (Figure 1B) was constructed by the display of the SP94 peptide on the outer surface of the pfFn nanocage (Figure 1A) by the genetic engineering approach. The flexible linker is important for recombinant proteins to keep their own biological activities. To optimize the HCC-targeting property of HccFn, we constructed the recombinant HccFn by linking the C terminus of the SP94 peptide (SFSIIHTPILPL) to the N terminus of pfFn through two types of flexible amino acid sequences (long linker: GGGSGGGGSGGGS and short linker: GGGGS), named L-HccFn and S-HccFn, respectively. We also displayed the reverse peptide of SP94 (LPLIPTHIISFS) on the pfFn nanocage via a long linker, named R-L-HccFn. All recombinant proteins were expressed in *Escherichia coli* (*E. coli*). After purification, the recombinant proteins were analyzed by sodium dodecyl sulfate-polyacrylamide gel electrophoresis (SDS-PAGE) (Figure S1) and size-exclusion chromatography (SEC) (Figure S2). All proteins were composed of 24 subunits according to molecule weight determined by SEC (Figure S2). Among them, S-HccFn, L-HccFn, and R-L-HccFn proteins exhibited a significant increase in subunit molecule weight than that of native pfFn. Transmission electron microscopy (TEM) (Figure 1D) and dynamic light scattering (DLS) (Figure 1E) analyses revealed that the L-HccFn, R-L-HccFn, and S-HccFn proteins exhibit a monodispersed self-assembled spherical cage-like structure as well as a well-defined morphology. The native pfFn, S-HccFn, L-HccFn, and R-L-HccFn protein nanocages exhibited an average radius of 6.7, 7.5, 8.6, and 8.4 nm in solution, respectively.

The HCC tumor cell line, HepG2, was used to evaluate the cellular binding activity of HccFn nanocages to HCC cells. Fluorescein isothiocyanate (FITC)-labeled native pfFn, S-HccFn, L-HccFn, and R-L-HccFn nanocages were incubated with HepG2 cells in vitro. Confocal laser scanning microscopy (CLSM) results revealed that S-HccFn, L-HccFn, and R-L-HccFn nanocages specially bound to the membrane of HepG2 cells within 30 min, whereas native pfFn exhibited no binding to HepG2 cells (Figure 1F). The binding affinity was determined by flow cytometry (FCM). As shown in Figure 1C, S-HccFn, L-HccFn, and R-L-HccFn nanocages exhibited a higher affinity (K_d = 1−100 nM) for HepG2 cells than that of the free SP94 peptide (K_d > 600 nM). Among recombinant proteins, the L-HccFn nanocage exhibited the highest affinity for HepG2 ($K_d \leq 1$ nM). The high binding affinity of L-HccFn is likely due to the self-assembly of the ferritin nanocage, which enables multivalent peptide recruitments to interact with the receptors on HepG2 cells as well as the ability of the long flexible linker to efficiently display the SP94 peptides on the surface of the ferritin nanocage. Thus, we chose L-HccFn as an effective HCC-targeting nanocage for the following studies, and we refer to L-HccFn as HccFn nanocage in the following main text.

Taken together, we successfully synthesized an HCC-targeted HccFn nanocage, which exhibited a well-defined morphology and monodispersity.

2.2. Synthesis and Characteristics of HccFn(Co_3O_4) Nanozymes. To biomimetically synthesize cobalt nanozymes, we employed the as-prepared pfFn (Figure 2A) and HccFn (Figure 2D) nanocage as templates. According to the biomineral synthesis process of ferritin,[28] Co^{2+} ions entered into the cavity of ferritin nanocages via the hydrophilic channels. Then, H_2O_2 was added at 65 °C to accelerate the oxidation and nucleation of cobalt ions. After cobalt loading and oxidation, a well-defined cobalt oxide core with an average diameter of 5.7 nm was synthesized within the native pfFn protein shell (Figure 2C) and an average diameter of 6.3 nm was synthesized within the HccFn protein nanocage (Figure

DOI: 10.1021/acsami.8b20942
ACS Appl. Mater. Interfaces 2019, 11, 9747−9755

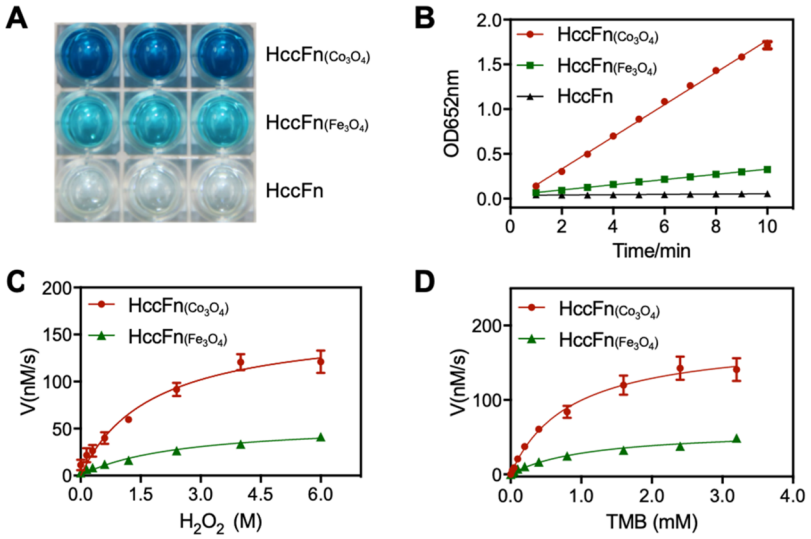

Figure 3. HccFn(Co_3O_4) nanozymes exhibit higher peroxidase-like activity than HccFn(Fe_3O_4) nanozymes. (A) Characterization of peroxidase-like activity of HccFn(Co_3O_4) and HccFn(Fe_3O_4). The same concentration (0.25 μM) of HccFn(Co_3O_4), HccFn(Fe_3O_4), and HccFn was respectively mixed with reaction solution [800 mM H_2O_2, 0.2 mg/mL TMB (Sigma), and 0.2 M sodium acetate buffer (pH 4.5)]. After 10 min, TMB was oxidized and blue-colored products were produced. The three parallel wells represent three repeats. (B) The curves showed absorbance variation with time at 652 nm wavelength in different catalytic reaction systems. The samples contained 800 mM H_2O_2, 0.2 mg/mL TMB (Sigma), and 0.2 M sodium acetate buffer (pH 4.5) with the same concentration (0.25 μM) of HccFn(Co_3O_4), HccFn(Fe_3O_4), and HccFn. (C,D) Kinetic analysis of HccFn(Co_3O_4) nanozymes with H_2O_2 (C) or TMB (D). For C, the TMB concentration was 800 μM, whereas the H_2O_2 concentration varied. For D, the H_2O_2 concentration was 2400 mM, whereas the TMB concentration varied.

Table 1. Kinetic Parameters of HccFn(Co_3O_4) and HccFn(Fe_3O_4) Nanozymes[a]

	[E] (M)	substrate	K_M (M)	V_{max} (M s^{-1})	K_{cat} (s^{-1})	K_{cat}/K_m (M^{-1} s^{-1})
HccFn(Co_3O_4)	4.7×10^{-8}	TMB	0.84	1.83×10^{-7}	3.90	4.64
HccFn(Co_3O_4)	4.7×10^{-8}	H_2O_2	1.77	1.62×10^{-7}	3.45	1.95
HccFn(Fe_3O_4)	2.3×10^{-7}	TMB	1.12	6.01×10^{-8}	0.26	0.23
HccFn(Fe_3O_4)	2.3×10^{-7}	H_2O_2	2.48	5.63×10^{-8}	0.24	0.10

[a] [E] is the nanozyme concentration, K_M is the Michaelis constant, V_{max} is the maximal reaction velocity, and K_{cat} is the catalytic constant, where $K_{cat} = V_{max}/[E]$ and the K_{cat}/K_M value represents the catalytic efficiency of the nanozymes.

2F). Cryo-electron microscopy (cryo-EM) images showed that Co_3O_4 cores were indeed synthesized in the cavity of native pfFn (Figure S3A) and HccFn nanocages (Figure S3B). The data of X-ray diffraction (XRD) confirmed that the crystalline form of biomimetically synthesized Co_3O_4 cores in the cavity of HccFn was identical with that of Co_3O_4 nanozymes (Figure S4). In addition, the encapsulating of Co_3O_4 nanozymes did not affect the self-assembled spherical cage-like structure and monodispersed state of native pfFn (Figure 2B) and HccFn (Figure 2E). DLS results further confirmed that the native pfFn(Co_3O_4), HccFn(Co_3O_4) nanozymes were monodispersed with an outer diameter of ~15 nm (Figure S5A) and 17 nm (Figure S5B) in phosphate-buffered saline (PBS, pH 7.4), respectively. Moreover, we synthesized HccFn(Fe_3O_4) nanozymes as control by iron loading and oxidation inside the HccFn nanocages.

Taken together, we successfully synthesized HccFn(Co_3O_4) nanozymes by employing HccFn nanocages as templates.

2.3. HccFn(Co_3O_4) Nanozymes Exhibit Higher Peroxidase-like Activity than That of HccFn(Fe_3O_4) Nanozymes. It has been reported that Co_3O_4 nanozymes exhibit higher peroxidase-like activity than that of Fe_3O_4 nanozymes.[17] Thus, we next investigated whether protein nanocage-encapsulated Co_3O_4 nanozymes possess higher peroxidase-like activity than encapsulated Fe_3O_4 nanozymes. Figure 3A shows that HccFn(Co_3O_4) catalyzed the oxidation of peroxidase-like substrate 3,3′,5,5′-tetramethylbenzidine (TMB) in the presence of H_2O_2 to give a stronger blue-colored product than that of HccFn(Fe_3O_4). The peroxidase-like activity comparison experiment between HccFn(Co_3O_4) and HccFn(Fe_3O_4) nanozymes is shown in Figure 3B, clearly indicating that a great improvement in peroxidase-like activity was achieved by employing HccFn(Co_3O_4) nanozymes as catalysts.

Both HccFn(Co_3O_4) and HccFn(Fe_3O_4) exhibited the typical Michaelis−Menten kinetics for H_2O_2 and TMB substrates, respectively. As shown in Table 1, the K_M values of HccFn(Co_3O_4) nanozymes for both TMB and H_2O_2 were lower than that of HccFn(Fe_3O_4) nanozymes, indicating that HccFn(Co_3O_4) nanozymes possess an apparently higher affinity to both substrates of TMB and H_2O_2. In addition, the V_{max} and K_{cat} of HccFn(Co_3O_4) nanozymes for both TMB and H_2O_2 were also higher than those of HccFn(Fe_3O_4) nanozymes (Table 1). Correspondingly, the K_{cat}/K_M, which reflects the catalytic efficiency of an enzyme for a given substrate, was compared to analyze the catalytic activity difference between HccFn(Co_3O_4) and HccFn(Fe_3O_4) nanozymes. The data showed that the K_{cat}/K_M for substrate TMB of HccFn(Co_3O_4) nanozymes was more than 20-fold higher than that of HccFn(Fe_3O_4) nanozymes (Table 1). Also, the K_{cat}/K_M for substrate H_2O_2 of HccFn(Co_3O_4) nanozymes was almost 20-fold higher than that of HccFn(Fe_3O_4) nanozymes (Table

DOI: 10.1021/acsami.8b20942
ACS Appl. Mater. Interfaces 2019, 11, 9747−9755

1). The kinetic assays indicate that HccFn(Co_3O_4) nanozymes exhibit intrinsic higher affinity for its substrate TMB and H_2O_2, as well as significant higher catalytic efficiency than that of HccFn(Fe_3O_4) nanozymes.

Above all, these results indicate that HccFn(Co_3O_4) nanozymes exhibit a much higher peroxidase-like activity compared to HccFn(Fe_3O_4) nanozymes. The HccFn protein shell, without a mineral core, exhibited no peroxidase-like activity (Figure 3B). Thus, the mineral core determines the peroxidase-like activity of the HccFn-based nanozymes (Figure 3A,B). Moreover, HccFn(Co_3O_4) nanozymes exhibited excellent stability. After being stored in PBS buffer for 2 months, the size distribution and peroxidase-like activity of HccFn(Co_3O_4) had no change (Figures S6 and S7). Taken together, HccFn(Co_3O_4) nanozymes exhibit higher peroxidase-like activity than HccFn(Fe_3O_4) nanozymes.

2.4. HccFn(Co_3O_4) Nanozymes Specifically Recognize and Visualize HCC Tissues. On the basis of our findings that HccFn nanocages specifically bound to HCC cells (Figure 1), we developed a novel HccFn(Co_3O_4) nanozyme-based IHC approach, aiming for rapid HCC diagnosis.

HccFn(Co_3O_4) nanozymes possess intrinsic peroxidase-like activity which catalyzes the oxidation of peroxidase substrate DAB to produce a deep-brown colorimetric reaction (Figure 4A). Moreover, the oxidation of cobalt ions in HccFn

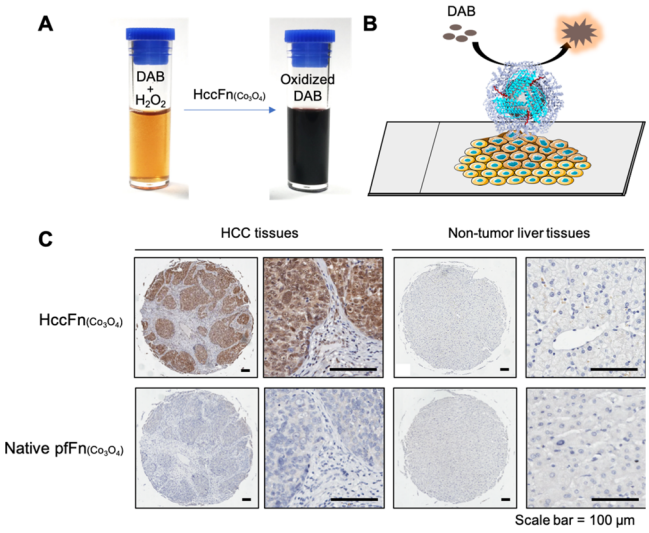

Figure 4. HccFn(Co_3O_4) nanozymes specifically recognize and visualize clinical HCC tissues. (A) HccFn(Co_3O_4) nanozymes showed peroxidase-like activity and catalyzed the oxidation of peroxidase substrate diaminobenzidine (DAB) to produce colorimetric reaction. (B) Schematic diagram of the HccFn(Co_3O_4)-based IHC approach. (C) HccFn(Co_3O_4)-based IHC staining (top row) and native pfFn(Co_3O_4)-based IHC staining (bottom row) of HCC tissues and nontumor liver tissues.

nanocages did not affect the binding ability of HccFn(Co_3O_4) nanozymes to HCC cells (Figure S8). As shown in Figure 4B, HccFn(Co_3O_4) nanozymes specifically bound to HCC tissues and gave a deep-brown colorimetric reaction in the presence of DAB and H_2O_2. Native pfFn(Co_3O_4) was used as control to compare its tumor-binding specificity and staining quality with our HccFn(Co_3O_4) nanozyme-based method in clinical HCC tissue specimens and nontumor liver tissue specimens. As shown in Figure 4C, HccFn(Co_3O_4) nanozymes specifically recognized and visualized HCC tissues, whereas native pfFn(Co_3O_4) could not distinguish tumor cells from normal tissues. Moreover, the staining intensity (SI) of HccFn-(Co_3O_4) nanozymes in HCC tissues was much stronger than that of native pfFn(Co_3O_4). In addition, HccFn(Co_3O_4) staining of nontumor liver tissues was minimal, which indicated the specificity of tumor detection by the HccFn-(Co_3O_4) nanozymes. Thus, HccFn(Co_3O_4) nanozymes were capable of specifically recognizing and visualizing HCC tissues.

2.5. HccFn(Co_3O_4) Nanozyme-Based HCC Diagnostic Method. To evaluate the validity of the HccFn(Co_3O_4) nanozyme-based HCC diagnostic method, we carried out the following histological staining experiments by using clinical HCC tissue specimens. As shown in Figure 5A, HccFn-(Co_3O_4) nanozymes specifically targeted and visualized tumor cells, whereas they scarcely stained nontumor liver cells. These results verified the feasibility of our HccFn(Co_3O_4) nanozyme-based HCC diagnostic method.

To evaluate the potential clinical application of the HccFn(Co_3O_4) nanozyme as a diagnostic agent for clinical HCC tissue specimens, we screened 424 clinical HCC tissue samples and 345 paired adjacent noncancerous samples by HccFn(Co_3O_4) nanozyme-based histological staining.

First, we analyzed the difference of HccFn(Co_3O_4) nanozyme staining results between HCC cancer tissues and paired adjacent nontumorous tissues. HccFn(Co_3O_4) nanozymes only slightly stained nontumorous liver tissues with a positive rate of 20.9% (72/345). In the positive nontumorous liver specimens, only 5.6% (4/72) showed strong staining, whereas 22.2% (16/72) were moderate-stained and 72.2% (52/72) were weak-stained (Figure 5B, Table S2). Meanwhile, HccFn(Co_3O_4) nanozymes showed stronger staining in HCC tumor tissues than in nontumorous tissues, and a clear distinction was seen between cancer cells and adjacent liver tissues as represented in Figure 5A. The sensitivity of HccFn(Co_3O_4) nanozyme staining to distinguish HCC tumor cells from nontumorous tissues was 63.4% (269/424) (Figure 5B, Table S1).

Next, we analyzed the correlation between HccFn(Co_3O_4) staining in tumor specimens and clinicopathological features of HCC patients. The frequency of positive staining increased with tumor differentiation degree of HCC (P value = 0.0246, χ-square test) (Figure 5C), as the positive rate was 50% (24/48) in well-differentiated (I) tissues, 65.7% (159/242) for moderate-differentiated (II) tumors, and 65.1% (84/129) for poor-differentiated (III) tissues, respectively. Among the positive staining specimens, the frequency of strong staining also increased (P value = 0.0115, χ-square test), as 14.5% (7/48), 16.9% (41/242), and 30.2% (39/129) for well-, moderate- and poor-differentiated specimens, respectively (Table S2). Similarly, the positive rate and intensity were also associated with tumor invasion (T) (P value < 0.0001, χ-square test) (Figure 5D). The frequency of positive staining was 32.4% (11/34) for T1 specimens, 59.5% (78/131) for T2, and 64.5% (58/90) for T3, and 100% (3/3) for T4. The frequencies of strong (P value < 0.0001, χ-square test) and moderate (P value < 0.0001, χ-square test) staining rate were also increased with tumor invasion (Table S3).

In addition, Kaplan–Meier survival analysis was used to analyze the overall survival of 144 HCC patients segregated by the immune response score (IRS) of HccFn(Co_3O_4). The mean follow-up was more than 5 years. As shown in Figure 5E, the HCC patients whose specimens were strongly stained (18.75%, 27/144) showed a poorer overall survival than those

DOI: 10.1021/acsami.8b20942
ACS Appl. Mater. Interfaces 2019, 11, 9747–9755

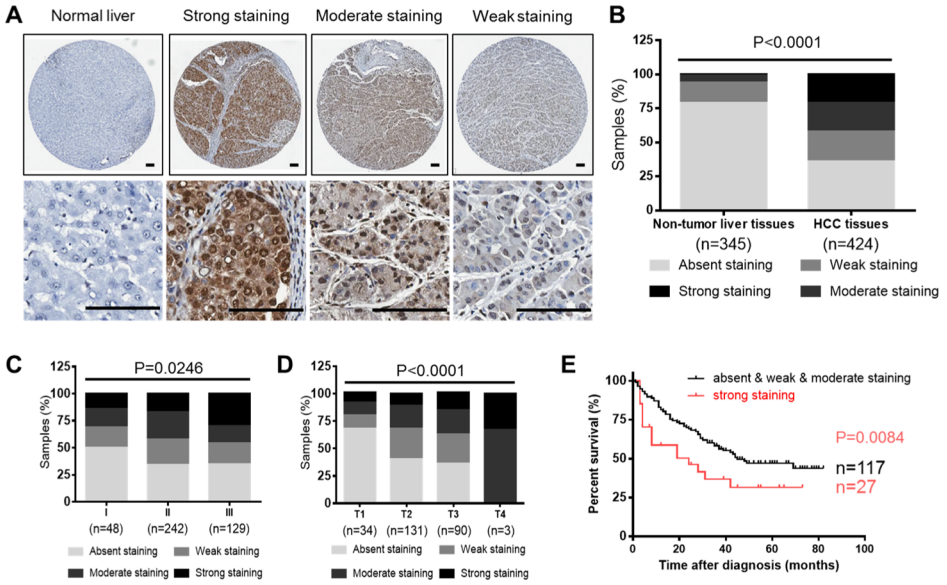

Figure 5. HCC diagnosis in clinical specimens using HccFn(Co_3O_4) nanozymes. (A) IHC staining of HccFn(Co_3O_4) in tissue microarrays derived from HCC patients. Binding activities of HccFn(Co_3O_4) were determined based on the SI (dark-brown reaction product). Scale bar, 100 μm. (B) Staining analysis of HccFn(Co_3O_4) to nontumor liver tissues and HCC tissues. Total HccFn(Co_3O_4) SI of HCC tissues was significantly stronger than that of nontumor liver tissues, χ-square test, $P < 0.0001$. (C) Distribution of HccFn(Co_3O_4) SI in clinical specimens derived from 419 HCC patients at different tumor differentiations. Overall, the HccFn(Co_3O_4) score correlated with tumor differentiation degree, χ-square test, $P = 0.0246$. Differentiation degree I, well-differentiated; differentiation degree II, moderate-differentiated; differentiation degree III, poor-differentiated HCC tissues. (D) Distribution of HccFn(Co_3O_4) SI in clinical specimens derived from 258 HCC patients at different tumor invasions (T). Overall, HccFn(Co_3O_4) SI correlated with T, χ-square test, $P < 0.0001$. (E) Kaplan–Meier plot of overall survival of 144 patients with HCC segregated by binding activities of HccFn(Co_3O_4). Overall, HccFn(Co_3O_4) staining score correlated with survival time after diagnosis, log-rank test, $P = 0.0084$.

with non-strong staining (absent & weak & moderate staining account for 81.25%, 117/144) patients (P value = 0.0084, <0.05, log-rank test).

3. DISCUSSION AND CONCLUSIONS

In this study, we biomimetically synthesized a novel ferritin-based nanozyme HccFn(Co_3O_4), and evaluated its potential application in clinical HCC diagnosis. HccFn(Co_3O_4) nanozymes possess monodispersity and HCC-targeting ability, exhibiting potential superiority in biomedical applications. Employing the HccFn(Co_3O_4) nanozyme-based HCC diagnostic method, we successfully distinguished clinical HCC tissues from normal tissues with a sensitivity of 63.5% and specificity of 79.1%, which is comparable with that of the clinically used HCC-specific marker AFP.[27] Moreover, the HccFn(Co_3O_4) nanozyme-based method is a one-step, time-saving way that can be potentially used in intraoperative pathological diagnosis. In addition, the diagnosis results of the HccFn(Co_3O_4) nanozyme-based IHC method on clinical HCC tissues correlated with parameters of HCC patients, which are valuable for prognostic diagnosis of HCC patients. In view of the specific HCC targeting ability of SP94, it is well worth identifying its receptor. Therefore, HccFn(Co_3O_4) nanozymes are promising reagents for HCC prognostic diagnosis.

Previously, we reported that iron-encapsulated HFn NPs (M-HFn) specifically target and visualize tumor tissues.[11] The M-HFn nanozyme-based tumor diagnostic method possesses a significant advantage over traditional antibody-based IHC staining. It is a one-step staining, which needs only one agent, and 0.5 h, whereas the antibody-based IHC method[29] needs two or three agents, and more than 4 h. The receptor of M-HFn in tumor cells is TfR1, which is overexpressed in various kinds of tumors. However, the pathological diagnosis of different clinical tumors with prognostic information needs more types of biomarkers. Thus, the M-HFn-based diagnosis method cannot satisfy the needs of prognostic diagnosis of certain types of tumor.

Here, we report a novel HccFn(Co_3O_4) nanozyme-based diagnosis method, which specifically recognizes HCC tissues via the HCC-targeting ability of SP94. Instead of chemical modification, we used the genetic engineering approach to construct the gene of HccFn by linking the sequence of the SP94 peptide to the N terminus of the ferritin. The advantages of a genetic engineering method are that it provides ease of synthesis and complete control over the structure with identical numbers of ligands. Owing to the self-assembly property of ferritin, we displayed 24 SP94 peptides on the outer surface of the pfFn nanocage to form eight bunches of SP94-trimers, which may further improve the bind affinity of the SP94 peptide to HCC cells.

We used ferritin isolated from *P. furiosus* (pfFn) to replace human heavy-chain ferritin (HFn) considering its heat stable ability[30] and non-TfR1 targeting to avoid the targeting interference with the SP94 peptide. Also, we encapsulated the Co_3O_4 nanozyme into the nanocage of pfFn, instead of the Fe_3O_4 nanozyme, creating a new HccFn(Co_3O_4) nanozyme which possesses higher peroxidase-like activity. Importantly, we first report that the Co_3O_4 nanozyme can be successfully synthesized inside the pfFn. Taken together, we synthesized a novel ferritin-based nanozyme HccFn(Co_3O_4), and developed a novel HccFn(Co_3O_4) nanozyme-based HCC diagnosis method.

Elucidating the catalytic mechanisms of Co_3O_4 nanozymes and Fe_3O_4 nanozymes may help us better understand the reason behind why HccFn(Co_3O_4) nanozymes exhibit higher

DOI: 10.1021/acsami.8b20942
ACS Appl. Mater. Interfaces 2019, 11, 9747–9755

peroxidase-like activity than HccFn(Fe_3O_4). The higher redox potential of Co^{3+}/Co^{2+} (1.30 V) in the Co_3O_4 nanozyme compared to that of Fe^{3+}/Fe^{2+} (0.771 V) in the Fe_3O_4 nanozyme may be the leading cause of the different peroxidase-like activities of HccFn(Co_3O_4) and HccFn(Fe_3O_4) nanozymes.[17] In addition, the interaction of inorganic nanomaterials with amino acid residues on the inner surface of the HccFn protein shell may produce more catalytic-active sites and substrate-binding sites.[31] The different interactions of the Co_3O_4 core and the Fe_3O_4 core with amino acid residues may also contribute to the higher peroxidase-like activity of the HccFn(Co_3O_4) nanozyme than that of HccFn(Fe_3O_4).

In the initial report of SP94, Lo et al. employed the M13 phage to display SP94 and developed a standard anti-M13 phage antibody-HRP-based immunoassay method for clinical HCC detection.[18] The positive rate of this method to detect HCC was 61.3% (19 of 31). Here, employing the pfFn nanocage to display SP94 and the Co_3O_4 nanozyme to replace the HRP-labeled antibody, we achieved a sensitivity of 63.5% and specificity of 79.1% with more than 400 clinical HCC specimens. More importantly, we also demonstrated that the HccFn(Co_3O_4) nanozyme is capable of prognostic diagnosis of HCC. Thus, the ferritin-based nanozyme is a promising nanoprobe for clinical tumor diagnosis, which is comparable to, even better than, antibody-HRP-based routine IHC methods.

Using ferritin as a template to synthesize a nanozyme is an efficient approach to synthesize a nanozyme in a controlled manner. Under mild reaction conditions, we synthesized the Co_3O_4 core in the HccFn nanocages with uniform size distribution, high biocompatibility, and high peroxidase-like activity. Ferritin-based nanozymes should greatly speed up the progress of developing nanozymes for biomedical applications. Moreover, low substrate specificity is a disadvantage of nanozymes compared with natural protein enzymes because of lacking of specific binding sites with specific substrate.[32] Therefore, designing new nanozymes with high substrate specificity will be a big challenge. Through genetic or chemical modification of ferritin nanocages, we may easily improve the substrate specificity of ferritin-based nanozymes.

In addition, ferritin is endowed with different targeting abilities by genetic or chemical modifying with targeting molecules. Thus, we may further develop ferritin-based Co_3O_4 nanozymes for pathology diagnosis of other types of diseases.

In conclusion, this study demonstrated that ferritin-based nanozyme HccFn(Co_3O_4) is a promising prognosis nanoprobe for prognostic diagnosis of HCC, which possesses the advantages of HCC-specific targeting ability, monodispersity, high peroxidase-like activity, thermal stability, low-cost, and time-saving. Ferritin-based nanozymes provide an efficient platform for targeting modification and size-controllable synthesis of nanozymes.

4. MATERIALS AND METHODS

4.1. Vector Construction, Protein Biosynthesis, and Purification. The gene-encoding peptide SP94 was constructed according to the amino acid sequence provided by Lo et al.[18] The amino acid sequence of pfFn was obtained from NCBI (NCBI reference sequence: WP_011011871.1). We constructed HccFn by linking the sequence of pfFn to the C terminus of the SP94 through two types of flexible amino acid sequences (long linker: GGGSGGGGSGGGS and short linker: GGGGS), named as L-HccFn, and S-HccFn, respectively. We also constructed R-L-HccFn by linking the sequence of pfFn to the C terminus of the reverse sequence of the SP94 peptide through the GGGSGGGGSGGGS linker. The genes of L-HccFn, S-HccFn, and R-L-HccFn were synthesized by Invitrogen. Then, the genes were subsequently cloned into the *E. coli* expression vector pET22b(+) plasmid (Novagen) with the *Nde*I and *Bam*HI restriction sites.

To produce the HccFn nanocage, the expression vector HccFn-pET22b(+) was transformed into *E. coli* Transetta (DE3) (TransGen Biotech). The HccFn protein was expressed in *E. coli* where it self-assembled into the 24-subunit nanocage. The transformed *E. coli* cells grew overnight in LB (Luria-Bertani) liquid medium with 100 mg/L ampicillin. Then, HccFn protein production was induced by isopropyl-β-D-thiogalactoside (0.8 mM, Sigma-Aldrich), and cells were incubated for an additional 8 h at 30 °C. After the incubation, *E. coli* cells were harvested by centrifugation at 4000*g* for 30 min and the pellets were resuspended in Tris buffer (20 mM Tris, pH 8.0). The resuspended *E. coli* cells were fragmented by a high-pressure homogenizer and centrifuged at 12 000*g* for 30 min. The supernatant was heated at 80 °C for 20 min to denature and precipitate most *E. coli* proteins. The HccFn protein was subsequently separated by ion-exchange chromatography on Q-Sepharose Fast Flow (GE Healthcare). Finally, the HccFn protein was purified by SEC on a Superdex 200 10/300 GL column (GE Healthcare). The concentration of HccFn was determined in triplicate by the bicinchoninic acid (BCA) protein assay kit (Pierce) using bovine serum albumin (BSA) as the standard. The typical yield of HccFn was 30 mg per 1 L patch.

4.2. Biophysical Characterization of Native pfFn and HccFn Nanocages. The prepared native pfFn and HccFn nanocages were characterized using TEM and DLS.

4.2.1. Transmission Electron Microscope. For TEM observation, the native pfFn and HccFn nanocage samples (20 μL, 0.1 mg/mL) were embedded in a Plasma Cleaner HPDC32G-treated copper grid and stained with 1% uranyl acetate for 1 min, then imaged with an JEM-1400 80 kV TEM (JEOL, Japan).

4.2.2. Dynamic Light Scattering. The native pfFn and HccFn protein samples (100 μL, 0.25 mg/mL) were prepared in PBS buffer. DLS analysis was performed using DynaPro Titan with a temperature-controlled microsampler (Wyatt Technology) at 25 °C.

4.3. Labeling of the HccFn Nanocage. The preparation of FITC-HccFn was according to the protocol provided by Sigma. In brief, dissolve the FITC (Sigma-Aldrich) in anhydrous dimethyl sulfoxide at 1 mg/mL, then add 50 μL of FITC solution to 2 mg/mL HccFn solution in 1 mL of carbonate/bicarbonate buffer (100 mM carbonate, pH 9.0). The mixture was incubated at 4 °C overnight. The FITC-conjugated HccFn was concentrated by centrifugation at 12 000*g* for 5 min, and the buffer was exchanged with PBS in a Vivaspin-4 Centrifugal Concentrator (MWCO 100 kDa, Sartorius) by centrifugation at 10 000*g* for 20 min, repeat eight times. The dye concentration of FITC or FITC-HccFn was determined by UV−vis spectroscopy (NanoDrop 2000, Thermo Fisher Scientific). The protein concentration was measured by the BCA protein assay kit (Pierce) using BSA as the standard.

4.4. Cell Line and Cell Culture. The human HCC cell line HepG2 was obtained from American Type Culture Collection. HepG2 cells were cultured in RPMI-1640 medium (Sigma-Aldrich) containing 10% fetal calf serum (Sigma-Aldrich), penicillin (100 U/mL, Sigma-Aldrich), and streptomycin (100 μg/mL, Sigma-Aldrich) at 37 °C with 5% CO_2. Cells were cultured in T-75 flasks (Corning) and passaged by trypsin−ethylenediaminetetraacetic acid digestion twice a week.

4.5. Cell-Binding Assays. The binding activities of the native pfFn and HccFn nanocage to HepG2 cells were performed on a FACSCalibur (Becton Dickinson) FCM system and CLSM.

4.5.1. Flow Cytometry. To perform the binding analysis, 100 μL of detached HepG2 cell suspensions (2.5×10^6 cells/mL) were incubated with 1 μg/mL of FITC-native pfFn or FITC-HccFn or FITC-HccFn(Co_3O_4) for 45 min at 4 °C in PBS containing 0.5% BSA. After three washes in cold PBS, cells were analyzed immediately using a FACSCalibur FCM system.

4.5.2. Confocal Laser Scanning Microscopy. HepG2 cells were cultured in 35 mm confocal dishes (Corning). When the cell density

DOI: 10.1021/acsami.8b20942
ACS Appl. Mater. Interfaces 2019, 11, 9747−9755

was over 90%, the cells were washed with PBS two times, and blocked in 5% normal goat serum for 45 min at 37 °C. Then, cells were incubated with 1 μg/mL of FITC-native pfFn or FITC-HccFn for 1 h at 37 °C in 5% normal goat serum. Cells were then washed three times with PBS and fixed in 4% cold formaldehyde in PBS for 10 min at room temperature. After washing with PBS, the nuclei of cells were stained by 4′,6-diamidino-2-phenylidole (DAPI, 1 μg/mL, Roche Applied Science) for 10 min at room temperature. The confocal dishes were examined with a CLSM (Olympus FluoView FV-1000, Tokyo, Japan).

4.6. Preparation and Characterization of HccFn(Co_3O_4) Nanozymes. HccFn protein shells were used as reaction templates to synthesize Co_3O_4 nanozymes according to the method reported by Fan et al.[33] Briefly, a degassed solution of HccFn protein (1 mg/mL in 100 mM NaCl) was added to a jacketed reaction vessel under N_2. The temperature of the reaction vessel was kept at 65 °C and the pH was titrated to 8.5. Cobalt(II) nitrate hexahydrate ($Co(NO_3)_2{\cdot}6H_2O$) was added as a cobalt source at a rate of 100 Co/(protein·min) to attain a theoretical loading factor of 5000 Co molecules per protein. Simultaneously, freshly prepared H_2O_2 was added at a stoichiometric equivalent of 1:3 H_2O_2/Co^{2+} as an oxidant. The reaction was considered complete 5 min after the addition of cobalt and H_2O_2. Sodium citrate was added to chelate any free cobalt. The synthesized HccFn(Co_3O_4) nanozymes were centrifuged to remove the aggregated nanozymes and then dialyzed against PBS overnight. The concentration of HccFn(Co_3O_4) nanozymes was assumed to be the same as that of the HccFn protein and was determined using a BCA protein assay kit (Pierce). Purified HccFn(Co_3O_4) nanozymes were obtained with a yield of >90%.

Cryo-EM analysis of native pfFn(Co_3O_4) nanozymes and HccFn-(Co_3O_4) nanozymes:

Approximately 3.0 μL aliquots of 1 mg/mL native pfFn(Co_3O_4) nanozyme and HccFn(Co_3O_4) nanozyme samples were applied to freshly glow-discharged Quantifoil (300 mesh R1.2/1.3) holey carbon grids. After removing the excess solution with filter paper, the grids were plunged rapidly into a liquid ethane bath cooled with liquid nitrogen using the semiautomatic EFI Vitrobot Mark IV with a blotting force of level −1 and blotting time of 0.5 s at 6 °C, 100% humidity. The images were collected on a Titan Krios G3 with a K2 camera positioned post a GIF quantum energy filter (Gatan, Inc.) in super resolution mode. Each micrograph (40 frames) was exposed for 4.48 s at a dose rate of 6 e/pixel/s. The pixel size at the object scale was 0.65 Å (nominal magnification 215 K), and the defocus ranges from 0.7 to 1.3 μm.

4.7. Staining of Clinical Specimens. Paraffin-embedded tissue sections were deparaffinized by washing twice in xylene for 10 min and then hydrated progressively using an ethanol gradient (100, 95, 80, 70, 60, 0%). Endogenous peroxidase activity was quenched by incubation with 3% H_2O_2 in methanol for 15 min. After being washed with ddH_2O, the tissue sections were boiled in 10 mM citrate buffer (pH 6.0) in a pressure cooker for 2.5 min, then cooled to room temperature, and blocked with 5% goat serum in PBS for 1 h at 37 °C, washed, and then incubated with HccFn(Co_3O_4) nanozymes (1 mg/mL) for 1 h at 37 °C, and then rinsed in PBS. Then, freshly prepared DAB was added to the tissue sections for color development. All samples were counterstained with hematoxylin (blue stain). The stained sections were analyzed under a panoramic scanning microscope (Zeiss).

The staining results were assessed by IRS, which was determined as a product of percentage of positive cells (PP) and SI. IRS = the score of PP × the score of SI. The SI was scored as 0 = negative, 1 = weak, 2 = moderate, and 3 = strong intensity. In addition, the percentage of positive stained cells was scored as 0 = no positive cells detectable, 1 = <1/3 of the cells, 2 = 1/3−2/3 of the cells, and 3 = >2/3 of the cells. The patients were then divided into four grades according to IRS as follows, IRS = 0 was determined "negative", "weak staining" was considered as IRS = 1 or 2, IRS = 3 or 4 was regarded as "moderate staining", and IRS = 6 or 9 were classified as "strong staining". Two independent pathologists who were blind to all clinical information scored all specimens.

4.8. Peroxidase Activity Test. A peroxidase activity test was carried out on HccFn(Co_3O_4) and HccFn(Fe_3O_4) nanozymes at room temperature. HccFn(Co_3O_4), HccFn(Fe_3O_4), or HccFn at 0.25 μM was mixed with 800 mM H_2O_2 in 0.2 M sodium acetate buffer (pH 4.5), using 0.2 mg/mL TMB (Sigma) as the substrate. Color reactions were recorded 15 min after addition of the substrate TMB.

Kinetic analysis of HccFn(Co_3O_4) nanozymes with H_2O_2: HccFn(Co_3O_4) at 0.047 μM or HccFn(Fe_3O_4) at 0.23 μM was mixed with 800 mM TMB in 0.2 M sodium acetate buffer (pH 4.5); then, H_2O_2 gradients (0, 0.15, 0.3, 0.6, 1.2, 2.4, 4, 6 M) were added to start the reaction.

Kinetic analysis of HccFn(Co_3O_4) nanozymes with TMB: HccFn(Co_3O_4) at 0.047 μM or HccFn(Fe_3O_4) at 0.23 μM was mixed with 2400 mM H_2O_2 in 0.2 M sodium acetate buffer (pH 4.5); then, TMB gradients (0, 0.15, 0.3, 0.6, 1.2, 2.4, 4, 6 M) were added to start the reaction.

■ ASSOCIATED CONTENT

Supporting Information

The Supporting Information is available free of charge on the ACS Publications website at DOI: 10.1021/acsami.8b20942.

SDS-PAGE analysis of native pfFn and HccFn; SEC analysis of native pfFn and HccFn; cryo-EM images of native pfFn(Co_3O_4) nanozymes and HccFn(Co_3O_4) nanozymes; XRD analysis of the Co_3O_4 nanozymes; DLS analysis of native pfFn(Co_3O_4) nanozymes and HccFn(Co_3O_4) nanozymes; curves showed absorbance variation with time at 652 nm wavelength in HccFn-(Co_3O_4) nanozymes catalytic reaction systems; FCM analysis of the binding activities of FITC labeled native pfFn, HccFn and HccFn(Co_3O_4) to HepG2 cells; histological analysis and statistical result of HccFn-(Co_3O_4) nanozyme staining of non-tumor liver tissues and HCC tissues (PDF)

■ AUTHOR INFORMATION

Corresponding Authors

*E-mail: fankelong@ibp.ac.cn (K.F.).
*E-mail: haochunyi@bjmu.edu.cn (C.H.).
*E-mail: yanxy@ibp.ac.cn (X.Y.).

ORCID

Kelong Fan: 0000-0001-6285-1933
Xiyun Yan: 0000-0002-7290-352X

Author Contributions

‖B.J. and L.Y. contributed equally to this work.

Notes

The authors declare no competing financial interest.

■ ACKNOWLEDGMENTS

We thank Jingnan Liang for technical support in TEM imaging at the Core Facility of Equipment, Institute of Microbiology. We thank the cryo-EM platform and the School of Life Sciences of PKU for cryo-EM data collection. We thank Dr. Guopeng Wang, Dr. Zhenxi Guo, Prof. Ning Gao for their help in the cryo-EM experiment and discussion. This work was financially supported by the National Natural Science Foundation of China (nos. 31871005, 31530026), Chinese Academy of Sciences under grant no. YJKYYQ20180048, the Strategic Priority Research Program (XDPB29040101), and the Key Research Program of Frontier Sciences (no. QYZDY-SSW-SMC013), Chinese Academy of Sciences.

DOI: 10.1021/acsami.8b20942
ACS Appl. Mater. Interfaces 2019, 11, 9747−9755

REFERENCES

(1) Gao, L.; Zhuang, J.; Nie, L.; Zhang, J.; Zhang, Y.; Gu, N.; Wang, T.; Feng, J.; Yang, D.; Perrett, S.; Yan, X. Intrinsic Peroxidase-Like Activity of Ferromagnetic Nanoparticles. *Nat. Nanotechnol.* **2007**, *2*, 577−583.

(2) Gao, L.; Yan, X. Nanozymes: An Emerging Field Bridging Nanotechnology and Biology. *Sci. China Life Sci.* **2016**, *59*, 400−402.

(3) Gao, L.; Fan, K.; Yan, X. Iron Oxide Nanozyme: A Multifunctional Enzyme Mimetic for Biomedical Applications. *Theranostics* **2017**, *7*, 3207−3227.

(4) Fan, K.; Xi, J.; Fan, L.; Wang, P.; Zhu, C.; Tang, Y.; Xu, X.; Liang, M.; Jiang, B.; Yan, X.; Gao, L. In Vivo Guiding Nitrogen-Doped Carbon Nanozyme for Tumor Catalytic Therapy. *Nat. Commun.* **2018**, *9*, 1440.

(5) Li, A. P.; Yuchi, Q. X.; Zhang, L. B. Ferritin: A Powerful Platform for Nanozymes. *Prog. Biochem. Biophys.* **2018**, *45*, 193−203.

(6) Lee, L. A.; Niu, Z.; Wang, Q. Viruses and Virus-Like Protein Assemblies-Chemically Programmable Nanoscale Building Blocks. *Nano Res.* **2009**, *2*, 349−364.

(7) Truffi, M.; Fiandra, L.; Sorrentino, L.; Monieri, M.; Corsi, F.; Mazzucchelli, S. Ferritin Nanocages: A Biological Platform for Drug Delivery, Imaging and Theranostics in Cancer. *Pharmacol. Res.* **2016**, *107*, 57−65.

(8) Zhang, L.; Laug, L.; Münchgesang, W.; Pippel, E.; Gösele, U.; Brandsch, M.; Knez, M. Reducing Stress on Cells with Apoferritin-Encapsulated Platinum Nanoparticles. *Nano Lett.* **2010**, *10*, 219−223.

(9) Sun, C.; Yang, H.; Yuan, Y.; Tian, X.; Wang, L.; Guo, Y.; Xu, L.; Lei, J.; Gao, N.; Anderson, G. J.; Liang, X.-J.; Chen, C.; Zhao, Y.; Nie, G. Controlling Assembly of Paired Gold Clusters within Apoferritin Nanoreactor for in Vivo Kidney Targeting and Biomedical Imaging. *J. Am. Chem. Soc.* **2011**, *133*, 8617−8624.

(10) Iwahori, K.; Yoshizawa, K.; Muraoka, M.; Yamashita, I. Fabrication of Znse Nanoparticles in the Apoferritin Cavity by Designing A Slow Chemical Reaction System. *Inorg. Chem.* **2005**, *44*, 6393−6400.

(11) Fan, K.; Cao, C.; Pan, Y.; Lu, D.; Yang, D.; Feng, J.; Song, L.; Liang, M.; Yan, X. Magnetoferritin Nanoparticles for Targeting and Visualizing Tumour Tissues. *Nat. Nanotechnol.* **2012**, *7*, 459−464.

(12) Zhang, W.; Zhang, Y.; Chen, Y.; Li, S.; Gu, N.; Hu, S.; Sun, Y.; Chen, X.; Li, Q. Prussian Blue Modified Ferritin as Peroxidase Mimetics and Its Applications in Biological Detection. *J. Nanosci. Nanotechnol.* **2013**, *13*, 60−67.

(13) Zhang, Y.; Ardejani, M. S.; Orner, B. P. Design and Applications of Protein-Cage-Based Nanomaterials. *Chem.—Asian J.* **2016**, *11*, 2814−2828.

(14) Li, X.; Qiu, L.; Zhu, P.; Tao, X.; Imanaka, T.; Zhao, J.; Huang, Y.; Tu, Y.; Cao, X. Epidermal Growth Factor-Ferritin H-Chain Protein Nanoparticles for Tumor Active Targeting. *Small* **2012**, *8*, 2505−2514.

(15) Kwon, K. C.; Ko, H. K.; Lee, J.; Lee, E. J.; Kim, K.; Lee, J. Enhanced In Vivo Tumor Detection by Active Tumor Cell Targeting Using Multiple Tumor Receptor-Binding Peptides Presented on Genetically Engineered Human Ferritin Nanoparticles. *Small* **2016**, *12*, 4241.

(16) Liu, B.; Han, X.; Liu, J. Iron oxide nanozyme catalyzed synthesis of fluorescent polydopamine for light-up Zn2+detection. *Nanoscale* **2016**, *8*, 13620−13626.

(17) Dong, J.; Song, L.; Yin, J.-J.; He, W.; Wu, Y.; Gu, N.; Zhang, Y. Co3O4 Nanoparticles with Multi-Enzyme Activities and Their Application in Immunohistochemical Assay. *ACS Appl. Mater. Interfaces* **2014**, *6*, 1959−1970.

(18) Lo, A.; Lin, C.-T.; Wu, H.-C. Hepatocellular Carcinoma Cell-Specific Peptide Ligand for Targeted Drug Delivery. *Mol. Cancer Ther.* **2008**, *7*, 579−589.

(19) Jin, Y.; Yang, X.; Tian, J. Targeted polypyrrole nanoparticles for the identification and treatment of hepatocellular carcinoma. *Nanoscale* **2018**, *10*, 9594−9601.

(20) Xu, L.; Xu, S.; Wang, H.; Zhang, J.; Chen, Z.; Pan, L.; Wang, J.; Wei, X.; Xie, H. Y.; Zhou, L.; Zheng, S.; Xu, X. Enhancing the Efficacy and Safety of Doxorubicin Against Hepatocellular Carcinoma Through A Modular Assembly Approach: the Combination of Polymeric Prodrug Design, Nanoparticle Encapsulation, and Cancer Cell-Specific Drug Targeting. *ACS Appl. Mater. Interfaces* **2018**, *10*, 3229.

(21) Li, Y.; Hu, Y.; Xiao, J.; Liu, G.; Li, X.; Zhao, Y.; Tan, H.; Shi, H.; Cheng, D. Investigation of SP94 Peptide as A Specific Probe for Hepatocellular Carcinoma Imaging and Therapy. *Sci. Rep.* **2016**, *6*, 33511.

(22) Jin, Y.; Wang, K.; Tian, J. Preoperative Examination and Intraoperative Identification of Hepatocellular Carcinoma Using A Targeted Bimodal Imaging Probe. *Bioconjug. Chem.* **2018**, *29*, 1475−1484.

(23) Ashley, C. E.; Carnes, E. C.; Phillips, G. K.; Padilla, D.; Durfee, P. N.; Brown, P. A.; Hanna, T. N.; Liu, J.; Phillips, B.; Carter, M. B.; Carroll, N. J.; Jiang, X.; Dunphy, D. R.; Willman, C. L.; Petsev, D. N.; Evans, D. G.; Parikh, A. N.; Chackerian, B.; Wharton, W.; Peabody, D. S.; Brinker, C. J. The Targeted Delivery of Multicomponent Cargos to Cancer Cells by Nanoporous Particle-Supported Lipid Bilayers. *Nat. Mater.* **2011**, *10*, 389−397.

(24) Liang, M.; Fan, K.; Zhou, M.; Duan, D.; Zheng, J.; Yang, D.; Feng, J.; Yan, X. H-Ferritin-Nanocaged Doxorubicin Nanoparticles Specifically Target and Kill Tumors with A Single-Dose Injection. *Proc. Natl. Acad. Sci. U.S.A.* **2014**, *111*, 14900−14905.

(25) Fan, K.; Zhou, M.; Yan, X. Questions about Horse Spleen Ferritin Crossing the Blood Brain Barrier via Mouse Transferrin Receptor 1. *Protein Cell* **2017**, *8*, 788−790.

(26) Fan, K.; Jia, X.; Zhou, M.; Wang, K.; Conde, J.; He, J.; Tian, J.; Yan, X. Ferritin Nanocarrier Traverses the Blood Brain Barrier and Kills Glioma. *ACS Nano* **2018**, *12*, 4105−4115.

(27) Wan, H.-G.; Xu, H.; Gu, Y.-M.; Wang, H.; Xu, W.; Zu, M.-H. Comparison Osteopontin vs AFP for the Diagnosis of HCC: A meta-analysis. *Clin. Res. Hepatol. Gastroenterol.* **2014**, *38*, 706−714.

(28) Honarmand Ebrahimi, K.; Bill, E.; Hagedoorn, P.-L.; Hagen, W. R. The Catalytic Center of Ferritin Regulates Iron Storage via Fe(II)-Fe(III) Displacement. *Nat. Chem. Biol.* **2012**, *8*, 941−948.

(29) Shi, S. R.; Key, M. E.; Kalra, K. L. Antigen retrieval in formalin-fixed, paraffin-embedded tissues: an enhancement method for immunohistochemical staining based on microwave oven heating of tissue sections. *J. Histochem. Cytochem.* **1991**, *39*, 741−748.

(30) Tatur, J.; Hagen, W. R.; Matias, P. M. Crystal Structure of the Ferritin From the Hyperthermophilic Archaeal Anaerobe Pyrococcus Furiosus. *J. Biol. Inorg Chem.* **2007**, *12*, 615−630.

(31) Sun, H.; Zhou, Y.; Ren, J.; Qu, X. Carbon Nanozymes: Enzymatic Properties, Catalytic Mechanism, and Applications. *Angew. Chem., Int. Ed.* **2018**, *57*, 9224−9237.

(32) Liu, B.; Liu, J. Surface Modification of Nanozymes. *Nano Res.* **2017**, *10*, 1125−1148.

(33) Uchida, M.; Flenniken, M. L.; Allen, M.; Willits, D. A.; Crowley, B. E.; Brumfield, S.; Willis, A. F.; Jackiw, L.; Jutila, M.; Young, M. J.; Douglas, T. Targeting of Cancer Cells with Ferrimagnetic Ferritin Cage Nanoparticles. *J. Am. Chem. Soc.* **2006**, *128*, 16626−16633.

DOI: 10.1021/acsami.8b20942
ACS Appl. Mater. Interfaces 2019, 11, 9747−9755